Kinetic Characterization of Reductant Dependent Processes of Iron Mobilization from Endocytic Vesicles†

J. Abra Watkins,* James D. Altazan, Pam Elder, Cai-Yuan Li, Marco-Tulio Nunez,‡ Xue-Xiang Cui, and Jonathan Glass*

Department of Medicine, Hematology/Oncology Division, Center of Excellence for Cancer Research, Treatment, and Education, Louisiana State University Medical Center, 1501 Kings Highway, Shreveport, Louisiana 71130

Received June 28, 1991; Revised Manuscript Received April 3, 1992

ABSTRACT: The reductant dependence of iron mobilization from isolated rabbit reticulocyte endosomes containing diferric transferrin is reported. The kinetic effects of acidification by a H^+-ATPase are eliminated by incubating the endosomes at pH 6.0 in the presence of 15 μM FCCP to acidify the intravesicular milieu and to dissociate ^{59}Fe(III) from transferrin. In the absence of reductants, iron is not released from the vesicles, and iron leakage is negligible. The second-order dependence of rate constants and amounts of ^{59}Fe mobilized from endosomes using ascorbate, ferrocyanide, or NADH are consistent with reversible mechanisms. The estimated apparent first-order rate constant for mobilization by ascorbate is $(2.7 \pm 0.4) \times 10^{-3}$ s^{-1} in contrast to $(3.2 \pm 0.1) \times 10^{-4}$ s^{-1} for NADH and $(3.5 \pm 0.6) \times 10^{-4}$ s^{-1} for ferrocyanide. These results support models where multiple reactions are involved in complex processes leading to iron transfer and membrane translocation. A type II NADH dehydrogenase (diaphorase) is present on the endosome outer membrane. The kinetics of extravesicular ferricyanide reduction indicate a bimolecular–bimolecular steady-state mechanism with substrate inhibition. Ferricyanide inhibition of ^{59}Fe mobilization is not detected. Significant differences between mobilization and ferricyanide reduction kinetics indicate that the diaphorase is not involved in ^{59}Fe(III) reduction. Sequential additions of NADH followed by ascorbate or vice versa indicate a minimum of two sites of ^{59}Fe(III) residence; one site available to reducing equivalents from ascorbate and a different site available to NADH. Sequential additions using ferrocyanide and the other reductants suggest interactions among sites available for reduction. Inhibition of ascorbate-mediated mobilization by DCCD and enhancement of ferrocyanide and NADH-mediated mobilization suggest a role for a moiety with characteristics of a proton pore similar to that of the H^+-ATPase. These data provide significant constraints on models of iron reduction, translocation, and mobilization by endocytic vesicles.

Reduction of ferric iron by a transmembrane oxidoreductase has been suggested to be an important reaction in the overall process of iron absorption by reticulocytes, hepatocytes, and intestinal epithelia (Nunez et al., 1990; Thorstensen, 1988; Crane et al., 1985). Iron uptake by reticulocytes involves endocytosis of diferric transferrin [Fe(III)$_2$-Tf]transferrin receptor (R_{Tf})[1] complexes giving rise to endocytic vesicles which contain the proteins and enzymes required for iron release into the cytosol (Nunez et al., 1983, 1990; Nunez & Glass, 1985). Iron mobilization from isolated endocytic vesicles into the cytosol has been demonstrated in vitro and has been shown to require several reactions that are independent of the handling of Tf contained in endocytic vesicles (Nunez et al., 1990; Watkins et al., 1990).

In vitro, iron mobilization requires both acidification of the intravesicular space and reduction of Fe(III). Initially, ATP is required to provide an energy source for a proton-transporting ATPase (H^+-ATPase) which acidifies the intravesicular space. Acidification is necessary for dissociation of iron from transferrin (Nunez et al., 1990; Nunez & Glass, 1985; Glass & Nunez, 1986; Iacopetta & Morgan, 1983). Following iron dissociation from the Fe(III)$_2$–Tf–R_{Tf} complex, which occurs in the intravesicular space, reducing equivalents supplied by NADH, ascorbate, or ferrocyanide are required for iron reduction which allows Fe(II) mobilization by extravesicular carriers (Nunez et al., 1983, 1990). Although the requirement for ATP can be circumvented by suspending the vesicles in an acidic buffer (pH 6.0) in the presence of a protonophore, reducing equivalents are absolutely necessary (Nunez et al., 1990). The rate of iron dissociation from the Fe(III)$_2$–Tf–R_{Tf} complex is relatively rapid and coupled to the interior pH of the vesicle (Nunez et al., 1990). Subsequent processes including Fe(III) reduction, translocation across the membrane, and mobilization are either rate limiting or rate determining for isolated vesicles. Since it is not clear which of these three processes is rate determining, the kinetics of the NADH dehydrogenase oxidoreductases of endocytic vesicles were explored to further the understanding of iron transport mechanisms by reticulocytes.

Ferricyanide has been shown to serve as an adequate probe of the activity of the type II NADH dehydrogenase oxidoreductase (Sun et al., 1984; Wang, 1980). Determination of the concentration dependence of ferricyanide reduction on

† This work was supported by the National Institutes of Health Grant DK-37866 and National Science Foundation Grant INT-8715381.

* Address correspondence to these authors.

‡ Permanent address: Departmento de Bilogia, Facultad de Ciencias, Universidad de Chile, Casilla 653, Santiago, Chile.

[1] Abbreviations: NADH, nicotinamide adenine dinuleotide; dhI, type I NADH dehydrogenase oxidoreductase; Tf, transferrin; R_{Tf}, transferrin receptor; ATP, adenosine triphosphate; H^+-ATPase, vacuolar proton transporting ATPase; dhII, type II NADH dehydrogenase ferricyanide reductase; FCCP, carbonyl cyanide *p*-(trifluoromethoxy)phenylhydrazone; FITC, fluoroscein isothiocyanate; DCCD, *N,N'*-dicyclohexylcarbodiimide; PBS, phosphate-buffered saline (137 mM NaCl, 2.7 mM KCl, 8.1 mM Na_2HPO_4, 1.5 mM KH_2PO_4); HEPES, *N*-(2-hydroxyethyl)piperazine-*N'*-2-ethanesulfonic acid; EGTA, ethylene glycol bis(β-aminoethyl ether)-*N,N,N',N'*-tetraacetic acid; PMSF, phenylmethanesulfonyl fluoride; NEM, *N*-ethylmaleimide.

0006-2960/92/0431-5820$03.00/0

NADH, ferricyanide, the amount of endocytic vesicles, and pH is reported here and an ordered bimolecular–bimolecular steady-state mechanism with substrate inhibition is indicated, in agreement with previous observations (Wang, 1980) for a plasma membrane type II NADH oxidoreductase (dhII). In addition, the dependence of the observed iron mobilization rate on NADH, ferrocyanide, and ascorbate concentrations is examined, and several apparent first-order processes intrinsic to the endosomal membrane proteins are revealed. The role of a transmembrane electron transfer protein in processes leading to iron mobilization is shown to be significant, in contrast to kinetic analysis that indicate dhII is not involved. Overall, the observed kinetics and computed rate constants, providing insights into the mechanism(s) of iron reduction leading to translocation and mobilization, and the rate-limiting step(s) of iron transport by isolated vesicles are discussed. These results provide significant constraints on models of the molecular events leading to iron transport across endocytic membranes.

Experimental Procedures

Preparation of Endocytic Vesicles Containing [^{125}I,$^{59}Fe_2$]-Transferrin. Endocytic vesicles from rabbit reticulocytes were prepared as described previously (Nunez et al., 1990; Choe et al., 1987) with some modifications. Packed red cells (40–70% reticulocytes) were incubated at 37 °C for 5–7 min with 15 μM carbonyl cyanide *p*-(trifluoromethoxy)phenylhydrazone (FCCP) in phosphate-buffered saline (PBS) at a ratio of 10 mL of packed cells to 40 mL of buffer. The cell suspension was pelleted at 5000 rpm for 5 min in a Sorvall RC-5B centrifuge using a SS-34 rotor and incubated with 2 μM [^{125}I,$^{59}Fe_2$]Tf for 10 min at 37 °C followed by centrifugation at the same speed. The cells were incubated at 4 °C with iron-saturated plasma for 10 min and washed three times in PBS. Cells loaded with [^{125}I,$^{59}Fe_2$]Tf and FCCP were resuspended in elution buffer (10 mM HEPES–Tris buffer, 50 mM NaCl, 50 mM KCl, 1 mM $MgSO_4$, 1 mM EGTA, 0.04% PMSF, pH 7.0) and subjected to three cycles of freeze-thaw lysis using liquid nitrogen. Cell lysate was separated from plasma membrane and contaminating mitochondria by centrifugation for 30 min at 21 000 rpm using the Sorvall SS-34 rotor, and 10 mL of lysate was loaded onto a 50-mL Bio-Rad A-5M column equilibrated with elution buffer. Endocytic vesicles eluted in the void volume and were collected before hemoglobin eluted. Aggregated vesicles and particulate matter were removed by centrifugation at 21 000 rpm for 30 min in the SS-34 rotor. The FCCP was removed from the vesicles using 2% bovine serum albumin (BSA) in elution buffer, and the vesicles were pelleted by centrifugation at 27 000 rpm for 1.25 h in a Beckman L7-55 centrifuge using an SW-28 rotor. The vesicles were resuspended in elution buffer at pH 7.0. Unless indicated, all procedures were performed at 4 °C. Using these methods, isolated vesicles contained fully saturated transferrin on the basis of the $^{59}Fe/^{125}I$ ratio (Nunez et al., 1990). Typically, 1–3 mg of endocytic vesicle protein was obtained from 8–12 mL of packed reticulocytes.

Measurement of Intravesicular Acidification. Vesicles were prepared from reticulocytes incubated with FITC-labeled [^{125}I,^{59}Fe]Tf or FITC-Tf for these studies (Nunez et al., 1990). Acidification of the intravesicular space was determined from fluorescence quenching of the FITC-Tf or FITC-labeled [^{125}I,^{59}Fe]Tf inside the vesicles using an Aminco SLM SP-F-500C fluorescence spectrophotometer as previously described (Nunez et al., 1990). Excitation at 497 nm produced the FITC emission at 528 nm which was used to monitor pH-dependent quenching. Excitation at 450 nm produced an emission at 528 nm which did not exhibit pH-dependent quenching and was therefore used as a control for relative fluorescence intensity. Calibration curves of pH verses fluorescence intensity were generated for each preparation as described previously (Nunez et al., 1990) by equilibrating the vesicles to various pH values using either 0.2% Nonidet P-40 (NP-40) or 15 μM FCCP. Fluorescence quenching kinetics were converted to pH using the calibration curve for each preparation. Acidification rates and final pH achieved were observed to be identical for isotopically labeled and nonisotopically labeled FITC-Tf.

Determination of ^{59}Fe Dissociation from [^{125}I,^{59}Fe]-Transferrin. The dissociation of ^{59}Fe from [^{125}I,^{59}Fe]Tf in the vesicles was determined as previously described (Nunez et al., 1990) by the removal of a 500-μL aliquot of vesicles (100–200 μg of protein/mL) in pH 6.0 or 7.0 reaction buffer and addition of 50 μL of 2.0% NP-40 and 5.0 mM deferoxamine, pH 7.2, in order to solubilize the membrane and chelate any unbound iron. The solution was incubated for 1 h at 23 °C with goat anti-rabbit transferrin IgG (DAKO Immunological) followed by incubation with 100 μg of Protein G–agarose beads (Boeringer-Mannheim). The agarose beads were washed three times with 1 mL of ice-cold PBS, and the percent saturation of transferrin bound to the beads was determined from the (cpm ^{59}Fe)/(cpm ^{125}I) ratio of the beads relative to the ratio of 100% saturated transferrin used in the initial incubation with the reticulocytes (Glass et al., 1980). Using these methods, dissociation of iron from Tf was not observed prior to the addition of ATP at pH 7.0 or FCCP at pH 6.0, which indicated that the presence of EGTA and deferoxamine to the buffer did not significantly affect iron dissociation.

Determination of Mobilization of ^{59}Fe from Endocytic Vesicles. Vesicles containing [^{125}I,$^{59}Fe_2$]Tf were incubated at 37 °C in elution buffer under a variety of conditions including variations in NADH, ascorbate, ferrocyanide, and ferricyanide concentrations. Experiments were also performed to examine effects of variations of the buffer pH in the presence or absence of FCCP. Aliquots of the vesicle solution (usually 125–250 μL, containing a minimum of 10 μg of vesicle protein and 600 cpm of ^{59}Fe) were separated from the incubation solution containing mobilized ^{59}Fe by filtration through 0.22-μm Millipore GSWP filters pretreated with two 2-mL washes with ice-cold PBS and one 2-mL wash with 2% BSA in PBS at pH 7.0 on a Hoeffer FH 225V 10-place vacuum manifold. The ^{59}Fe and ^{125}I radioactivity retained on the filters was determined with a Pharmacia-LKB Compugamma 1282 γ counter. Retention of vesicles by the filters was greater than 95% as determined from the [^{125}I]Tf radioactivity of the filtrates. Mobilization of iron was determined from the decrease of the (cpm ^{59}Fe)/(cpm ^{125}I) ratio at defined incubation times relative to the (cpm ^{59}Fe)/(cpm ^{125}I) ratio at the initial (0 min) incubation time. Control experiments were performed without added reductant, FCCP, or ATP for each preparation at each time point to determine the percentage of radioactivity contributed by inside-out or broken vesicles. On rare occasions, 5–15% of the total [^{125}I,^{59}Fe]Tf appeared associated with inside-out or broken vesicles as indicated by measurements of [^{125}I]Tf radioactivity in the filtrate and an increasing (cpm ^{59}Fe)/(cpm ^{125}I) on the filter. Efforts to detect ^{59}Fe leakage or release from the isolated endosomes were unsuccessful. Experiments under oxygen, argon, nitrogen, or carbon monoxide gave identical results for iron mobilization.

Determination of NADH Dehydrogenase Oxidoreductase Activity. Reduction of ferricyanide was determined from the decrease in the 420-nm ferricyanide absorbance maxima

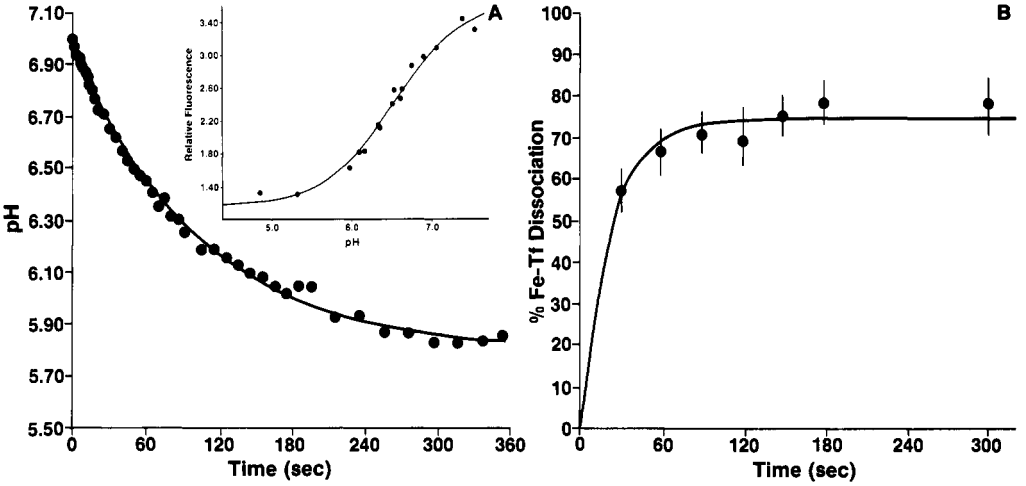

FIGURE 1: (A) Acidification of the intravesicular space of isolated endosomes equilibrated in pH 7.0 reaction buffer at 37 °C, as determined from the fluorescence quenching of FITC labeled transferrin following the addition of 1 mM ATP. (Inset to A) Titration of intravesicular FITC–transferrin fluorescence at 528 nm using the emission ratio for excitation at 493 nm relative to excitation at 450 nm with vesicle solutions containing 15 μM FCCP. (B) Kinetics of ^{59}Fe dissociation from ^{125}I labeled transferrin, as determined from immunoprecipitation, during acidification following the addition of 1 mM ATP under conditions identical to those in (A).

Table I: Effect of Reaction Conditions on Observed Iron Mobilization Rate Constants and Amounts of Iron Mobilized[a]

reductant	ATP (1 mM)	FCCP (15 μM)	pH_{out}	pH_{in}	k_{obs} (× 10^4 s^{-1})	percent mobilization
none	−	−	7.00	7.00	0	0
none	+	−	7.05	5.85	0.2 ± 2	3 ± 2
none	−	+	6.00	6.00	0	0
ascorbate	−	−	7.05	7.05	0	0
ascorbate	+	−	7.00	5.90	37.3 ± 3.3	55 ± 5
ascorbate	−	+	6.05	6.05	33.6 ± 3.1	56 ± 5
NADH	−	−	7.00	7.00	0	0
NADH	+	−	7.05	5.95	2.4 ± 0.7	30 ± 4
NADH	−	+	6.10	6.10	2.8 ± 0.5	28 ± 5
ferrocyanide	−	−	7.05	7.05	0	0
ferrocyanide	+	−	7.05	6.00	6.3 ± 0.7	44 ± 5
ferrocyanide	−	+	6.00	6.00	6.2 ± 0.8	43 ± 5

[a] Estimate ±SD for observed rate constants and percent mobilization using reductant concentrations of 1 mM ascorbate, 40 μM NADH, or 1 mM ferrocyanide in elution buffer at 37 °C. pH_{out} and pH_{in} are extravesicular and intravesicular pH, respectively, with standard deviations of ±0.07.

(Wang, 1980). Alternatively, the time dependence of the decrease in the 340-nm absorbance of NADH was determined when oxygen and/or Fe(III), originally on transferrin, was the primary acceptor. Spectral changes were monitored on a Beckman DU-70 or Hitachi U-3210 spectrophotometer. Observed spectral changes were consistent with expectations based on the extinction coefficients and a 2:1 ferricyanide: NADH reducing equivalent ratio. Observed rates were independent of vesicle concentration (0.01–4.0 mg of vesicle protein/mL). However, very low total vesicle protein concentration (less than 5 μg/mL) gave slower rates of ferricyanide reduction. Experiments under oxygen, argon, nitrogen, or carbon monoxide gave identical results for ferricyanide reduction.

Data Analysis. All kinetic data were linear out to five half-lives on semilogarithmic plots with no apparent kinetic heterogeneity that could not be ascribed to limitations in the sensitivity of the detectors. Rate constants were computed from single-exponential fits using the ENZFITTER program (Elsevier Biosoft). Second-order plots and double-reciprocal plots were also analyzed using the ENZFITTER program although some amplitude data were analyzed using the MathCAD program (MathSoft Inc.). All data are the average of measurements on at least three independent preparations.

RESULTS

Acidification and Iron Dissociation from Transferrin Is Rapid. Isolated vesicles containing FITC-labeled [^{59}Fe,^{125}I]Tf equilibrated in pH 7.0 reaction buffer (10 mM HEPES–Tris, 50 mM NaCl, 50 mM KCl, 1 mM $MgCl_2$, 1 mM EGTA) at 37 °C were able to acidify the intravesicular space and dissociate Fe from Tf following the addition of 1 mM ATP in pH 7.0 reaction buffer as shown in Figure 1. Both acidification and dissociation reached completion in less than 6 min with a final pH of about 6.0 ± 0.25 and with 75 ± 15% of the Fe dissociated from Tf. Dissociation was near maximal in about 100 s, at which time the intravesicular pH was about 6.2. Iron mobilization could not be detected under these conditions where reductants are absent (Table I). Under all conditions, the pH gradient could be dissipated by the addition of 1–5 μM monensin, FCCP, or nigericin. Preincubation of the vesicles with 50 μM *N*-ethylmaleimide (NEM) or *N,N'*-dicyclohexylcarbodiimide (DCCD) for 30 min completely inhibited both acidification and dissociation.

Iron Mobilization at pH 7.0 Using ATP and Mobilization at pH 6.0 Using FCCP Is Similar. The mobilization of ^{59}Fe from endocytic vesicles using ascorbate or NADH as reductants is much slower than the acidification and dissociation steps (Nunez et al., 1990). Efforts to detect ^{59}Fe leakage or release from the isolated endosomes were unsuccessful, indicating that vesicular ^{59}Fe is tightly bound before the addition of reductant. As shown in Table I, iron mobilization does not occur in the absence of reductants. In order to remove the possibility of complicating factors from ATP-dependent processes as well as the fact that ATP or ADP may serve as extravesicular chelators, mobilization experiments were conducted at 37 °C using pH 6.0 reaction buffer with 15 μM FCCP and compared to experiments using pH 7.0 reaction

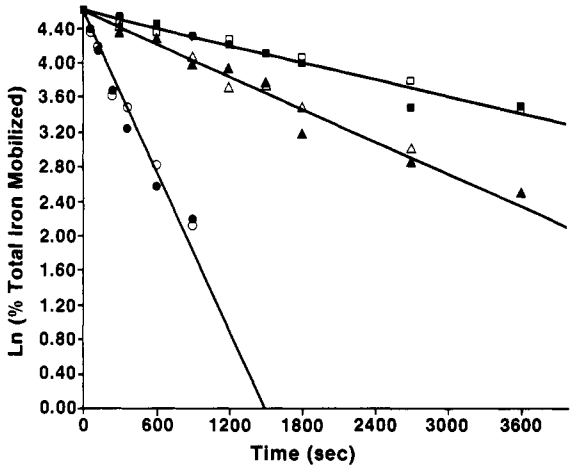

FIGURE 2: Typical kinetics of ^{59}Fe mobilization from endocytic vesicles at pH 7.0 with 1 mM ATP (solid symbols) and pH 6.0 with 15 μM FCCP (open symbols) using 1 mM ascorbate (circles), 40 μM NADH (squares), or 1 mM ferrocyanide (triangles) as reductant at 37 °C in reaction buffer.

buffer with 1 mM ATP. As shown in Figure 2, the kinetics of iron mobilization were virtually identical between these two sets of pH and buffer conditions and were consistent with pseudo-first-order kinetics for at least four half-lives. However, the kinetics for ascorbate show deviations from monophasic behavior near the end of the reaction. Although it is more rigorous to compute rate constants for ascorbate-mediated mobilization using biphasic kinetic models, the experimental significance and mechanistic assignments of rate constants are not clear in view of the complexities arising from transmembrane ascorbate transport (Escobar et al., 1992). In the interest of minimizing the complexity of the analysis, all pseudo-first-order data have been analyzed using monophasic kinetics.

Results of experiments conducted under oxygen, carbon monoxide, argon, or nitrogen were also identical to data shown in Table I as well as Figure 2 and indicate that oxygen or oxyradicals are not involved in the reactions. In addition, these results indicate that processes following iron dissociation from transferrin are reductant dependent and that it is possible to investigate iron mobilization without the mechanistic complications that might arise from the structural changes and possible conformational coupling resulting from ATP hydrolysis by the proton-pumping ATPase.

DCCD Has Significant Differential Effects on Iron Mobilization. The reaction of DCCD is to covalently bind to proton pores of the H^+-ATPase and possibly bind to a region of a transmembrane electron transfer protein with a structural motif similar to a proton pore (Vuokila & Hassinen, 1988). Using the pH 6.0 reaction buffer with FCCP, the effects of DCCD were examined in order to further explore possible roles the H^+-ATPase, or other proton pores, might have on events following Fe dissociation. Vesicles were equilibrated in pH 7.0 reaction buffer containing 50 μM DCCD at 25 °C for 30 min prior to a 1:10 or 1:20 dilution into pH 6.0 reaction buffer. These conditions should allow the reaction of DCCD with proton pores to be complete (Sun et al., 1987; Arai et al., 1987). The final intravesicular pH was measured to be 6.0 ± 0.1, which is well within the range for maximal Fe dissociation from Tf (Figure 1). The rates and amounts of Fe mobilization by 40 μM NADH were consistent with the values reported above, indicating DCCD has no effect on the apparent kinetics of the NADH-driven process. Both the rate and extent of mobilization by 1 M ascorbate were inhibited by about 47 ± 5%. In contrast, DCCD enhanced the rate and amount of ferrocyanide mediated mobilization by 28 ± 10% and 58 ± 13%, respectively. These results suggest that Fe mobilization may occur through different transit routes from Tf to the exterior of the vesicle and that proton pores may be involved.

Endocytic Vesicles Have a Type II NADH Dehydrogenase Oxidoreductase That Is Not Involved in Iron Mobilization. The kinetics of NADH-mediated ferricyanide reduction by dhII (also known as diaphorase) were studied in order to assess the possibility that Fe(III) reduction by dhII occurs on the extravesicular side of the endocytic membrane. Ferricyanide reduction is dependent on both NADH and ferricyanide concentrations. Using 200 μM ferricyanide in pH 7.0 reaction buffer at 37 °C, the NADH concentration dependence of apparent pseudo-first-order rate constants for reduction was consistent with a Michaelis–Menten mechanism with an apparent V_{max} of (1.3 ± 0.15) × 10^{-2} s^{-1} and K_m of 32 ± 13 μM, while, at pH 6.0, the apparent V_{max} was (1.0 ± 0.1) × 10^{-2} s^{-1} and K_m was 5.5 ± 1.5 μM (Figure 3A). The kinetics of ferricyanide reduction were observed to be independent of vesicle protein concentrations from 0.01 to 4 mg/mL, and no differences between activities were detected in the presence or absence of FCCP and/or ATP. In pH 6.0 reaction buffer, observed rates using 40 μM NADH were in a concentration range where second-order NADH concentration effects were

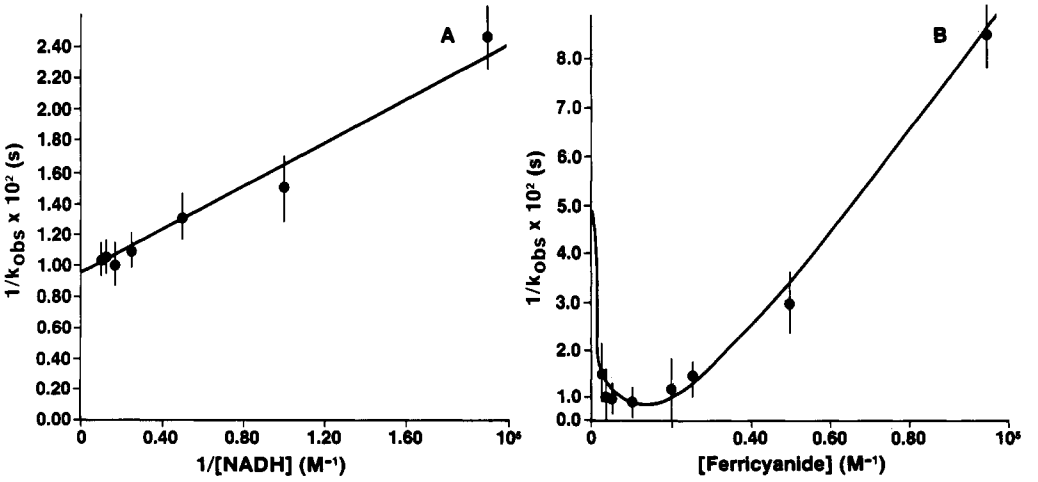

FIGURE 3: Second-order kinetics of type II NADH dehydrogenase ferricyanide oxidoreductase activity of endocytic vesicles at pH 6.0: (A) NADH concentration dependence at 200 μM ferricyanide; (B) ferricyanide concentration dependence at 40 uM NADH. Solid curves were computed using a V_{max} and K_m of 0.01 s^{-1} and 5.5 μM, respectively, for panel A. Solid curves for panel B were computed using K_{Ib} = 60 μM, K_{ma} = 64 μM, K_a = 64 μM, K_{mb} = 100 μM, and V_{max} = 0.07 s^{-1} with eq 2.

negligible as indicated by the apparent K_m. Under these conditions, the dependence of ferricyanide reduction on ferricyanide concentration was studied and found to exhibit hyperbolic behavior with significant inhibition at high concentrations (Figure 3B). These results are consistent with previous observations on dhII from human erythrocytes and support an ordered bimolecular–bimolecular steady-state mechanism with substrate inhibition as shown in (Wang, 1977, 1980)

$$\mathrm{EB} \overset{K_{Ib}}{\rightleftharpoons} \mathrm{E} + \mathrm{A} + \mathrm{B} \underset{k_{-1}}{\overset{k_1}{\rightleftharpoons}} \mathrm{EA} + \mathrm{B} \underset{k_{-2}}{\overset{k_2}{\rightleftharpoons}}$$

$$\mathrm{EAB} \underset{k_{-3}}{\overset{k_3}{\rightleftharpoons}} \mathrm{EPQ} \underset{k_{-4}}{\overset{k_4}{\rightleftharpoons}} \mathrm{EP} + \mathrm{Q} \underset{k_{-5}}{\overset{k_5}{\rightleftharpoons}} \mathrm{E} + \mathrm{P} + \mathrm{Q} \quad (1)$$

where A is NADH, B is ferricyanide, E is free enzyme, P and Q are oxidation–reduction products where the order of release is not known, and K_{Ib} is the dissociation constant for the inactive ferricyanide–dhII bimolecular complex. Dissociation of either ferricyanide or NAD^+ first is rapidly followed by dissociation of the other product giving rise to conditions where k_5 and k_{-5} are negligible. The data was adequately described by eq 2 derived from reaction 1, where K_{ma} and K_{mb} are the Michaelis–Menten constants for NADH and ferricyanide, respectively, and all other parameters are defined as in reaction 1 (Wang, 1980; Cleland, 1963; Segel, 1975):

$$\frac{1}{k_{obs}} = \frac{1}{V_{max}}\left(1 + \frac{IK_{ma}}{[A]} + \frac{K_{mb}}{[B]} + \frac{IK_aK_{mb}}{[A][B]}\right) \quad (2)$$

$$I = 1 + ([B]/K_{Ib})$$

$$K_{ma} = k_3k_4/k_1(k_3 + k_4)$$

$$K_{mb} = k_4(k_{-2} + k_3)/k_2(k_3 + k_4)$$

$$K_a = k_{-1}/k_1$$

From reaction 1, it was expected that ferricyanide should significantly inhibit Fe mobilization by NADH if dhII were involved in the Fe(III) reduction mechanism since ferricyanide reduction occurs at 10^{-2} s^{-1} while iron mobilization occurs at 10^{-4} s^{-1}. Mobilization experiments using 40 μM NADH were conducted using 100, 200, and 400 μM ferricyanide. Ferricyanide did not inhibit NADH-driven mobilization, suggesting that dhII is probably not involved in the reduction processes leading to Fe mobilization. However, the kinetics of ferricyanide reduction under these conditions are sufficient to produce ferrocyanide-mediated Fe mobilization by a reduction process involving a different electron transfer protein as described below.

Dependence of Iron Mobilization Rates and Extents on Ascorbate, Ferrocyanide, and NADH Concentrations. The second-order dependence of Fe mobilization on reductant concentrations was investigated using pH 6.0 reaction buffer with 15 μM FCCP at 37 °C in order to further elucidate differences among apparent reduction mechanisms or Fe translocation pathways. The reductant concentration dependence of apparent pseudo-first-order rate constants for Fe mobilization demonstrated a variety of apparent second-order and limiting first-order processes (Figure 4A–C). The apparent nonzero intercepts at very low reductant concentrations (0.5–1.0 μM) shown in Figure 4 are not artifacts since baseline levels of Fe transport are negligible when reductants are not present (Table I). Although Fe mobilization by ferrocyanide and NADH had different apparent kinetic mechanisms, the observed limiting rates at low NADH and high ferrocyanide concentrations were similar as were the observed limiting rates at high NADH and low ferrocyanide concentrations. In

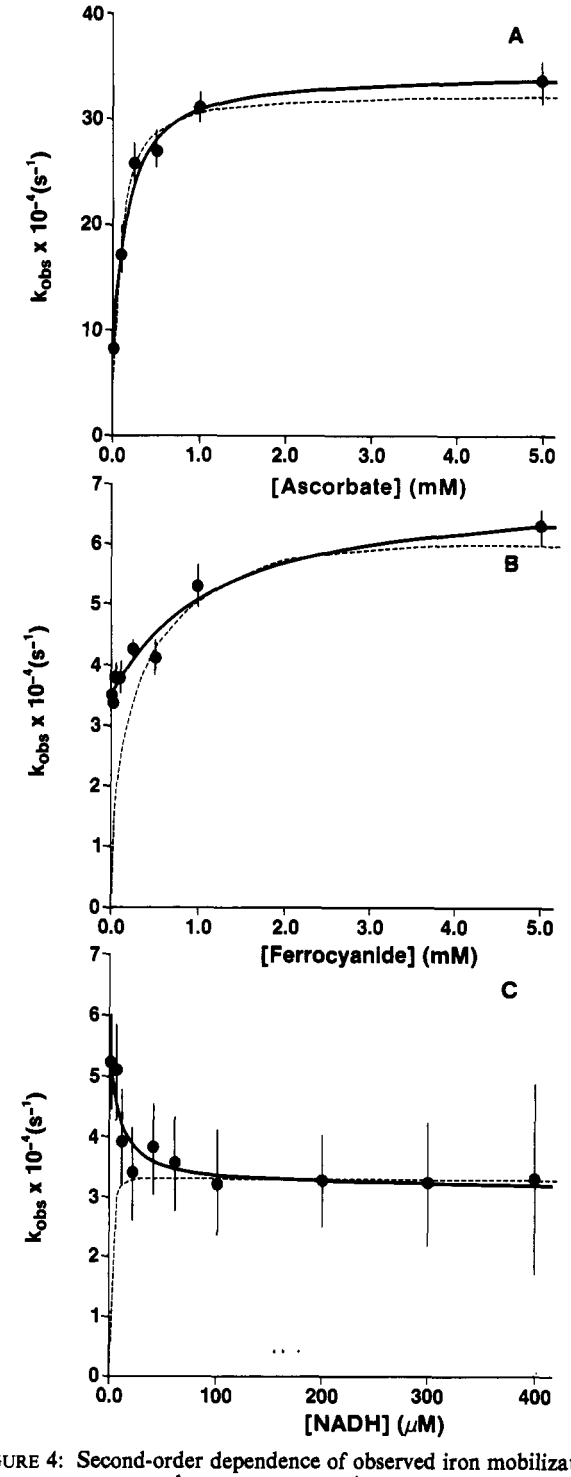

FIGURE 4: Second-order dependence of observed iron mobilization rate constants on reductant concentrations at pH 6.0, using the following reductants: (A) ascorbate, (B) ferrocyanide, and (C) NADH. Solid curves were computed using eqs 6 and 8 with parameters given in Table II. The dashed curves were computed using an irreversible two-step steady-state mechanism with V_{max} and K_m parameters given in Table II.

contrast, the observed limiting first-order rate at high ascorbate concentrations was almost an order of magnitude faster, revealing an additional relatively fast process not detected using the other reductants (Figure 4A–C). The amount of Fe mobilization was also dependent on reductant concentrations. Limiting amounts of approximately 50% of total vesicular Fe were mobilized by both ascorbate and ferrocyanide (Figure 5A,B). The amount of Fe mobilized by NADH was about 25% and was also dependent on NADH concentration (Figure

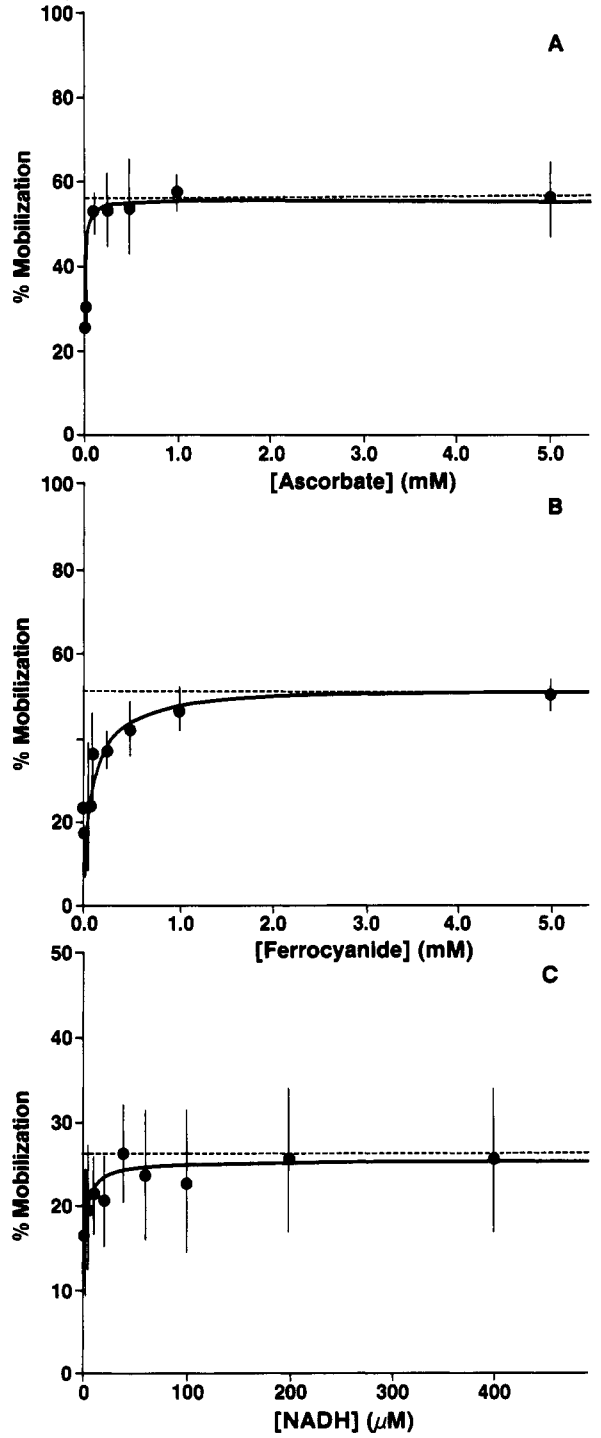

FIGURE 5: Second-order dependence of observed amounts of iron mobilized on reductant concentration at pH 6.0, using the following reductants: (A) ascorbate, (B) ferrocyanide, and (C) NADH. Solid curves were computed using eqs 7 and 9 with parameters given in Table II; dashed curves were predicted from steady-state mechanisms using the percent maximum mobilization parameters given in Table II.

5C). The rates and amounts of Fe mobilization by ascorbate and ferrocyanide could be adequately described by a reversible rapid equilibrium model derived from the kinetic mechanisms in reactions 3 and 4 (Frost & Pearson, 1953; Fersht, 1977):

$$R^- + Fe^{3+}i \underset{k_{sr}}{\overset{k_{rs}}{\rightleftharpoons}} R^-Fe^{3+}i \underset{k_{-t}}{\overset{k_t}{\rightleftharpoons}} R + Fe^{2+} \qquad (3)$$

where the first bimolecular step is fast, R^- is the reductant (ascorbate), Fe^{3+} is ferric iron at site i (different from Tf), and Fe^{2+} is mobilized ferrous iron. Since ascorbate is transported into the intravesicular space much faster than iron mobilization (Escobar et al., 1992), ascorbate is proposed to interact at an intravesicular iron binding site i. Although ferrocyanide-mediated mobilization is described by a similar rapid equilibrium mechanism, it is not transported into the endosome and must interact with a transmembrane electron transfer protein at the extravesicular surface as described by

$$R^- + (A)Fe^{3+}j \underset{k_{sr}}{\overset{k_{rs}}{\rightleftharpoons}} R^-(A)Fe^{3+}j \underset{k_{-p}}{\overset{k_p}{\rightleftharpoons}} R(A) + Fe^{2+} \qquad (4)$$

where the first bimolecular step is fast, R^- is the reductant (ferrocyanide), Fe^{3+} is ferric iron at site j (different from Tf and site i), (A) is an intermediate electron acceptor/donor of a transmembrane electron transfer protein, k_p and k_{-p} are rate constants for intermolecular or intramolecular configurational rearrangements, and Fe^{2+} is mobilized ferrous iron.

Mobilization rates and amounts using NADH were consistent with an isomer interconversion model derived from the mechanism in reaction 5 (Eigen & de Maeyer, 1963; Fersht & Requena, 1971; Fersht, 1977; Faller et al., 1991):

$$(A^*)Fe^{3+}j \underset{k_{a^*}}{\overset{k_a}{\rightleftharpoons}} (A)Fe^{3+}j + R^- \underset{k_{sr}}{\overset{k_{ra}}{\rightleftharpoons}} R(A) + Fe^{2+} \qquad (5)$$

where the second bimolecular step is fast, and $(A^*)Fe^{3+}j$ is ferric iron at site j which is unavailable for reduction until configurational rearrangements occur in (A*) leading to the R^- and (A) mediated reduction at site j which may not necessarily be bound to (A) at the time of rearrangement. In addition, site j does not necessarily have to be different from site i in reaction 3 or identical to site j in reaction 4.

Ascorbate-dependent kinetic parameters (Table II) were estimated using eq 6 derived from the conditions and mechanism of reaction 3, assuming $k_t + k_{-t}$ is much slower than $k_{sr}[R^-]Fe^{3+}i$ (Frost & Pearson, 1953; Fersht, 1977; Cantor & Schimmel, 1980):

$$k_{obs} = k_{-t} + \frac{k_t[R^-]}{K_d + [R^-]} \qquad (6)$$

$$K_d = k_{sr}/k_{rs}$$

where rate constants are defined according to reaction 3 and the reductant concentration $[R^-]$ is ascorbate. Based on the parameters computed using eq 6, an estimation of the apparent lower limits of reductant association (k_{rs}) and dissociation (k_{sr}) rates could be obtained from eq 7 derived from the time-independent term (Fox et al., 1974) using the conditions of reaction 3 for the mobilized Fe^{2+} product:

$$\%Mob = \frac{\%Mob_{max}k_{rs}k_t[R^-]}{bk_{obs}} \qquad (7)$$

$$b = k_{rs}[R^-] + k_{sr}$$

where %Mob is the percent of initial vesicular iron mobilized at a given reductant concentration, rate constants are defined according to reaction 3, k_{obs} is defined according to eq 6, and $\%Mob_{max}$ is the maximum amount of initial iron mobilized at high reductant concentrations. Estimates of the minimum values of k_{rs} and k_{sr} are given in Table II. Ferrocyanide-dependent kinetic parameters were estimated using expressions identical in form to eqs 6 and 7 except k_{rs}, k_{sr}, k_t, and k_{-t} were replaced by k_{ra}, k_{ar}, k_p, and k_{-p}, respectively.

Kinetic parameters determined for NADH-dependent mobilization were estimated using eq 8 derived from the condi-

Table II: Kinetic and Equilibrium Parameters Estimated from Rate and Amplitude Data[a]

estimated constant	ascorbate	NADH	ferrocyanide
V_{max} (s^{-1})	$(3.2 \pm 0.3) \times 10^{-3}$	$(3.6 \pm 1.2) \times 10^{-4}$	$(6.5 \pm 0.6) \times 10^{-4}$
K_m (M)	$(6.9 \pm 3.5) \times 10^{-5}$	$(2.5 \pm 2.0) \times 10^{-6}$	$(3.3 \pm 1.7) \times 10^{-7}$
K_d (M)	$(2.8 \pm 0.3) \times 10^{-5}$	$(8.6 \pm 0.3) \times 10^{-6}$	$(1.9 \pm 0.5) \times 10^{-4}$
$\%Mob_{max}$	$56 \pm 8\%$	$25 \pm 7\%$	$50 \pm 5\%$
k_t (s^{-1})	$(2.7 \pm 0.4) \times 10^{-3}$		
k_{-t} (s^{-1})	$(7.0 \pm 1.3) \times 10^{-4}$		
k_a (s^{-1})		$(3.2 \pm 0.3) \times 10^{-4}$	
k_{a*} (s^{-1})		$(2.4 \pm 0.4) \times 10^{-4}$	
k_p (s^{-1})			$(3.5 \pm 0.6) \times 10^{-4}$
k_{-p} (s^{-1})			$(3.4 \pm 0.4) \times 10^{-4}$
k_{rs} (M^{-1} s^{-1})	$>(1.0 \pm 0.2) \times 10^{3}$		
k_{sr} (s^{-1})	$>(2.8 \pm 0.3) \times 10^{-2}$		
k_{ra} (M^{-1} s^{-1})		$>(1.0 \pm 0.4) \times 10^{3}$	$>10 \pm 2$
k_{ar} (s^{-1})		$>(8.6 \pm 0.9) \times 10^{-3}$	$>(1.9 \pm 0.2) \times 10^{-3}$

[a] Estimate ±SD. Estimates of K_m and V_{max} were determined using a two-step irreversible Michaelis–Menten mechanism, K_d and all other rate constants were determined using eqs 6–9. Only lower limits (>) of rate constants for apparent bimolecular reactions are reported and are constrained by estimates of K_d. Percent maximum mobilization ($\%Mob_{max}$) was directly observed from amplitude data.

tions of reaction 5 assuming $k_{a*}(A)Fe^{3+}j + k_a(A^*)Fe^{3+}j$ is much smaller than $k_{ra}[R^-]$ (Eigen & de Maeyer, 1963; Fersht & Requena, 1971; Fersht, 1977; Faller et al., 1991):

$$k_{obs} = k_a + \frac{k_{a*}k_{ar}/k_{ra}}{K_d + [R^-]} \quad (8)$$

$$K_d = k_{ar}/k_{ra}$$

where rate constants are defined according to reaction 5. The apparent dissociation constant computed from eq 8 was used to constrain lower limits of the second-order rate constant by eq 9 using the time-independent term derived from the conditions of reaction 5 for the mobilized Fe^{2+} product (Frost & Pearson, 1953; Fox et al., 1974; Cantor & Schimmel, 1980; Faller et al., 1991):

$$\%Mob = \frac{\%Mob_{max}k_{ra}k_a[R^-]}{ck_{obs}} \quad (9)$$

$$c = k_{ra}[R^-] + k_{ar}$$

where the rate constants are defined according to reaction 5, k_{obs} is defined by eq 8, and $[R^-]$ is the NADH concentration.

Kinetic parameters used to compute the curves in Figures 4 and 5 are described in Table II. All of the data for rates and amounts could be adequately described by two-step reversible mechanisms based on conditions for rapid equilibrium for ferrocyanide and ascorbate or isomer interconversion for NADH. Two-step irreversible mechanisms using Michaelis–Menten formalisms were also used for analyzing the results as shown in Figures 4 and 5 with parameters given in Table II. Although these irreversible stationary-state mechanisms could describe the ascorbate rate data, significant deviations from linearity on double-reciprocal plots for all reductants were noted (graphs not shown). In addition, irreversible stationary-state mechanisms could not describe the amplitude data in Figure 5. Since the amount of iron mobilized decreases proportionally with decreasing reductant concentration, it was difficult to measure mobilization rates below reductant concentrations of 0.5–1.0 μM. These constraints prevented estimation of bimolecular rate constants that are more accurate than the lower limits reported in Table II. A linear approximation of the bimolecular rate constant ($k_{obs} = k[R^-]$; $k = k_{obs}/[R^-]$) gave rate constants on the order of 10^2–10^3 M^{-1} s^{-1}, which is within the range of the estimates given in Table II. Nevertheless, differences between apparent second-order rate constants for these three reductants indicated kinetic diversity among bimolecular reactions leading to reduction and translocation of Fe(III). In addition, none of the computed kinetic parameters are similar to parameters used for obtaining fits to the data for dhII in Figure 3, lending support to the proposal that dhII is not involved in Fe mobilization via reduction on the extravesicular surface (Nunez et al., 1990). Limiting apparent first-order rate constants detected by these reductants indicated a variety of processes intrinsic to the vesicular membrane proteins.

Effects of Sequential Additions of Reductants. The reaction of vesicles with 1 mM ascorbate was followed to completion, and additional Fe mobilization was observed when 40 μM NADH was added (Figure 6A). Additive effects on Fe mobilization were also observed when 40 μM NADH was added and the reaction was allowed to proceed to completion followed by the addition of 1 mM ascorbate. Under the conditions of these sequential addition experiments, the apparent rates and amounts of Fe mobilization by ascorbate and NADH were identical to those observed when only one or the other of the reductants was used. Similar results were obtained with ferrocyanide when used in combination with the other reductants (Figure 6B,C). Parameters in Table I were used to determine predicted curves for the kinetics of iron mobilization assuming the reductants affect independent sites. However, initial mobilization by NADH or ascorbate appeared to enhance the observed rate and amount of iron mobilization by ferrocyanide by 19 ± 10% and 25 ± 12% relative to predicted estimates, respectively. In addition, initial mobilization by ferrocyanide appeared to enhance the observed amount of iron mobilized by NADH by 20 ± 12% relative to predicted estimates. These results indicate that Fe(III) available for reduction resides at a minimum of two different sites; one site that can be reduced by equivalents from ascorbate and a different site that can be reduced by NADH. Overall, multicomponent oxidation–reduction reactions as well as intramolecular and intermolecular iron transfer equilibria are indicated.

Discussion

It has been proposed that processes following Fe dissociation from Tf include reaction, translocation, and mobilization (Nunez et al., 1983, 1990; Watkins et al., 1991). Most of the results reported here were determined using vesicles equilibrated in HEPES-buffered saline with 15 μM FCCP at pH 6.0, in order to isolate the kinetics of processes following dissociation for investigation of mechanisms of reduction and translocation. Near maximum levels of Fe dissociation from Tf were obtained at pH 6.0 as shown in Figure 1 and are consistent with our previous observations (Nunez et al., 1990).

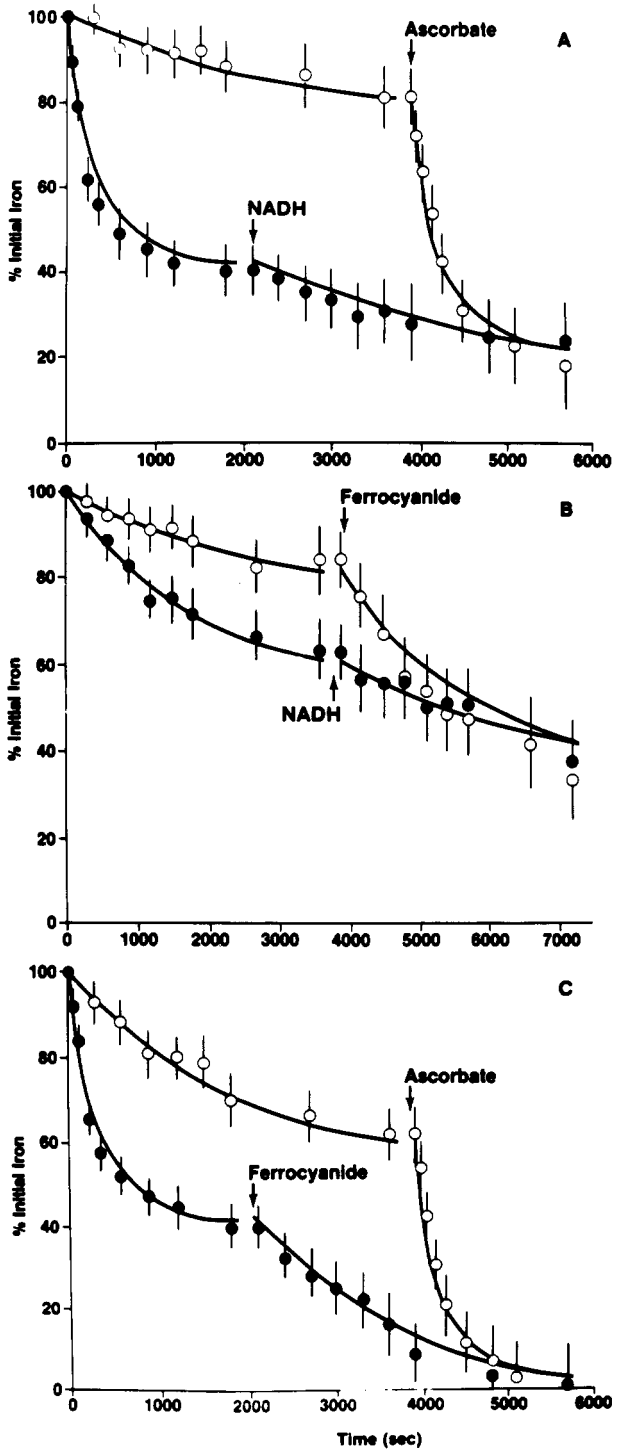

FIGURE 6: Iron mobilization kinetics of sequential additions of reductants at pH 6.0. Concentrations of reductants used were 40 μM NADH, 1 mM ascorbate, and 1 mM ferrocyanide added in the following sequences: (A) ascorbate first–NADH second (solid circles), NADH first–ascorbate second (open circles); (B) ferrocyanide first–NADH second (solid circles), NADH first–ferrocyanide second (solid circles); (C) ascorbate first–ferrocyanide second (solid circles), ferrocyanide first–ascorbate second (open circles). Data are the average of three independent experiments. Solid curves are kinetics predicted on the basis of data in Table II and Figures 4 and 5.

The observed rate and amount of reductant-mediated iron mobilization at pH 6.0 with FCCP are identical to observations at pH 7.0 with ATP (Figure 2). These results support previous proposals that Fe(III) reduction is kinetically distinct from the coupled processes of acidification and dissociation (Nunez et al., 1990; Watkins et al., 1991). In addition, it can be concluded that reactions involved in the processes of reduction, translocation, and mobilization are not affected by proton concentrations under these experimental conditions.

Under the reaction conditions, the Fe(III) dissociated from Tf has undergone redistribution to sites of the iron binding moieties involved in reduction as well as pathways leading to translocation and mobilization (Nunez et al., 1989, 1990). In the absence of reductants, iron is not released from vesicles at pH 6.0 with FCCP or at pH 7.0 with ATP over the 30–90 min time span required for a typical experiment. It is likely that Fe(III) remains bound to sites of the iron binding moieties of which the known ones have association constants of 3.63×10^9 and 3.96×10^8 M (Nunez et al., 1989). In addition, experiments performed under oxygen, nitrogen, argon, and carbon monoxide produce identical rates and amounts of iron mobilized. Overall, these controls indicate that iron is not "leaking" from the vesicles and that effects due to oxyradical-mediated reactions are negligible for these experimental conditions. Therefore, addition of reductants to the vesicle suspension results in reactions where the initial state is about 75% of total Fe(III) dissociated from transferrin and distributed among sites of the iron binding moieties and the final state is Fe(II) released from the extravesicular surface of the endosomes.

The reductant concentration dependence of iron mobilization rates provides information on the processes leading to reduction and translocation. Based on the results reported in Figures 3 and 4, it is likely that the actual mobilization step is faster than the rate at which reducing equivalents are delivered to Fe(III) in relative agreement with the values of kinetic parameters estimated from data obtained using intact reticulocytes (Watkins et al., 1991). Support for this proposal is found in data indicating that external nonmembrane permeable chelators do not increase the rate of mobilization (Nunez et al., 1990). Further, ferricyanide inhibition of mobilization is expected if Fe(II) residing on an extravesicular membrane site is released at a rate slower than oxidation by ferricyanide, which may be expected to be fast if outer sphere electron transfer processes are invoked. Overall, models where extravesicular Fe(III) reduction describes the amount of iron mobilized are inconsistent with results of the concentration dependence of observed mobilization rates, effects of high-affinity extravesicular chelators (Nunez et al., 1990), phenomena attributable to dhII, differences between mobilization kinetics of ascorbate and ferrocyanide, and observations of iron mobilization in intact reticulocytes (Watkins et al., 1991).

Concentration Dependence of Iron Mobilization. The second-order dependence of rates and amounts of iron mobilized (amplitudes) yields information on interactions of reductants with sites of electron transfer and reveals apparent first-order processes. The dissociation constants (K_d) can be estimated with reasonable confidence using reactions 3–5. In contrast, estimates of Michaelis–Menten constants (K_M) are determined with less confidence since stationary-state models do not provide adequate descriptions of both rate and amplitude data. Lower limits of the association and dissociation rate constants are estimated from the concentration dependence of amplitudes (Figure 5) as constrained by dissociation constants calculated from the rate dependence (Figure 4). These rate constants may be much larger than reported in Table II provided their ratios (k_{ar}/k_{ra} and k_{sr}/k_{rs}) are equivalent to estimates of K_d. On the basis of recent reports (Li et al., 1991b; Escobar et al., 1992), the oxidation of ascorbate at or near sites of Fe binding on the intravesicular surface can be proposed. Ferrocyanide and NADH are likely to reduce an electron acceptor moiety (A) of a transmembrane oxido-

reductase at the extravesicular membrane surface, which subsequently transfers electrons to the intravesicular surface for reduction of Fe(III) by an electron donor (D). Although these reactions may be detected, it is also likely that bimolecular processes are too fast to be resolved by the methods used here. For this case, the rate constants k_{ra}, k_{rs}, k_{ar}, and k_{sr} may represent other processes such as conformational adjustments involving the bound reductants or electron transfer per se. Despite these ambiguities regarding determination and assignment of rate constants relevant to bimolecular processes, the lower limit estimates are reported here in order to constrain models of endosomal iron transport. The computed parameters, irrespective of their model dependence, indicate that apparent bimolecular reactions involving these reductants are much faster than the rate-limiting first-order processes.

Estimation of the apparent first-order rate constants is reasonably accurate because these parameters are computed from observed rates at high reductant concentration as well as "apparent" intercepts at low reductant concentrations using reactions 3–5 (Figure 4). First-order rate constants for forward processes (k_t, k_a, k_p) are generally similar to estimates of V_{max}. The V_{max} estimates provide upper limits for first-order processes. However, the reversible mechanisms yield forward and reverse (k_{-t}, k_{a*}, k_{-p}) rate constants as well as provide descriptions of both rate and amplitude data. Although the most simple kinetic models are desired, much better descriptions are obtained using reversible mechanisms. These kinetic considerations suggest that processes preceding mobilization are reversible. On the basis of considerations requiring specific chemical or physical processes, events that may be kinetically significant include protein–protein interactions, conformational changes, intermolecular iron transfer, and/or long-range electron transfer reactions. In general, the computed apparent first-order rate constants determined from limiting conditions are likely to detect some of these molecular processes.

Assignment of the computed first-order rate constants to specific reactions is complicated by mechanistic considerations and error estimation. The similarity of the computed rate constant at low ascorbate concentration (k_{-t}) to the first-order rate constants for NADH and ferrocyanide can be interpreted in one of two ways depending on the quantitative significance of the errors estimated for the computed parameters. One possibility is that differences are not significant and can be attributed to errors arising from the measurements. Under these conditions, k_{-t} as well as the first-order rate constants determined from NADH and ferrocyanide reactions can be assigned to a process preceding iron translocation such as iron transfer between sites on the intravesicular surface or electron transfer from Fe(II) at an intravesicular site to donor/acceptor moieties. In contrast, if our error estimates are accurate, then it can be concluded that there are significant differences between the computed rate constants. In this case, it is reasonable to assign k_t and k_{-t} to forward and reverse rates of iron translocation, respectively. These assignments are supported by observations indicating that ascorbate directly reduces Fe(III) at sites on the intravesicular surface (Escobar et al., 1992). It is likely that events preceding iron translocation are detected by ferrocyanide and NADH since these reactions must begin by reduction of an electron donor/acceptor moiety on the extravesicular surface followed by multiple oxidation–reduction reactions which span the endosomal membrane. On the basis of reaction 5, k_{a*} might be assigned to conformational changes of a transmembrane electron transfer protein while k_{-p} might be assigned to configurational changes involving complexes of the membrane proteins or intermolecular iron transfer between sites on the intravesicular membrane surface. Based on these arguments and on the fact that k_a and k_p are nearly identical, it is likely that a single forward reaction for one of these processes is detected by the reactions of both ferrocyanide and NADH. Alternatively, differences among first-order rate constants may reflect various pathways of electron transfer involving transmembrane electron transfer proteins or differences between sites of iron binding and mechanisms of iron transfer between these sites. Although these assignments are speculative and tentative at this time, the potential for elucidating the relative significance of these processes is supported by these considerations and provides a basis for further study.

Amount of Iron Mobilized. The results obtained from sequential additions of reductants as well as the DCCD effects provide further support for at least two and possibly three Fe(III) sites that appear selectively mobilizable by NADH, ferrocyanide, and ascorbate, while enhancements of the rates and amounts may reveal interactions between the sites. The results suggest at least two independent pathways for the transfer of iron from the intravesicular binding sites to the site(s) where translocation occurs. The effects of DCCD in the absence of ATP at pH 6.0 with 15 μM FCCP indicate a role for a proton channel in iron mobilization. In view of the second-order dependence of mobilization, two different processes are explored using the reductants. Using 1 mM ascorbate, DCCD may affect the first-order translocation process per se or may disrupt iron binding to a site associated with a proton channel which may be involved in redistribution of iron to a site(s) whereby translocation occurs. Alternatively, DCCD may directly affect a transmembrane electron transfer protein which has a structural motif similar to a proton pore. Several recent reports indicate that DCCD binds to subunits of the mitochondrial NADH:ubiquinone oxidoreductase (type I NADH dehydrogenase oxidoreductase) and affects the kinetics but not the thermodynamics of electron and proton transfer activities (Honkakoski & Hassinen, 1986; Vuokila & Hassinen, 1988, 1989). In the event that DCCD binds to a transmembrane electron transfer protein, kinetic perturbation of intramolecular transmembrane electron transfer may result, giving rise to the observed effects on the amount of iron mobilized as well as the apparent rate. As discussed above, NADH- and ferrocyanide-mediated mobilization primarily detects the kinetics of NAD^+ dissociation, transmembrane electron transfer protein isomerization, and/or protein–protein interactions. Therefore, DCCD effects will be complicated by the molecular dynamics of the transmembrane electron transfer protein as detected by NADH in contrast to the rates of electron transfer and/or iron translocation as detected by ascorbate. In contrast, the enhancement of the amounts ferrocyanide- and NADH-mediated iron mobilization by DCCD may reflect a redistribution of iron to sites where reduction by electron donors on the intravesicular surface have greater accessibility. Additional studies, which are beyond the scope of this investigation, are necessary in order to fully elucidate the effects of DCCD as well as other inhibitors and are currently in progress in our laboratories. Nevertheless, the effects of DCCD as well as the sequential additions of reductants indicate the detection of a variety of intramolecular and/or intermolecular processes leading to the mobilization of iron from multiple intravesicular sites.

Molecular Mechanisms and Models of Iron Reduction and Translocation. Minimal models for the interactions leading to iron mobilization are given in Figure 7. Panel 1.a is the more simple model for electron and iron transport across the

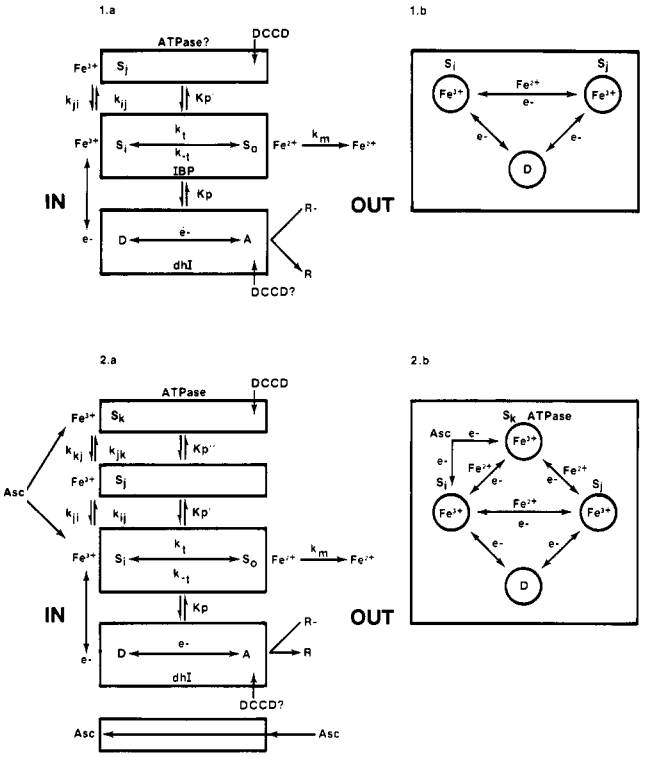

FIGURE 7: Possible models for molecular interactions leading to iron mobilization where the perspective is parallel to the plane of the membrane in panels 1a and 2a, where IN is the intravesicular space and OUT is the extravesicular solution, or perpendicular to the intravesicular membrane surface in panels 1b and 2b. Only processes after intravesicular acidification and iron dissociation from transferrin are shown with the initial state showing iron bound to a number of intravesicular sites (S_i, S_j, S_k) and the final state where reduced iron is mobilized from site S_o on the external surface of the vesicle. Roles for a transmembrane electron transfer protein (dhI), H^+-ATPase, iron binding and translocating protein (IBP), pathways of iron transfer, and pathways of electron transfer from the reductant (R^-) to an initial electron acceptor (A) leading to reduction of iron by an electron donor (D), as well as a possible ascorbate translocator are discussed in the text.

membrane involving a transmembrane electron transfer protein (a dhI-like enzyme) and at least two iron binding moieties S_i, a site on an iron channel, and S_j, a different site which may possibly be the H^+-ATPase proton channel (Li et al., 1991a,b). Figure 7, panel 2.a, is a more complex model with a transmembrane ascorbate transporter (Escobar et al., 1992) and an additional iron binding moiety. Transfer of electrons and ferrous iron among sites on the intravesicular surface are described in Figure 7 panel 1.b as well as panel 2.b, which includes a transmembrane ascorbate transporter leading to Fe(III) reduction by ascorbate on the intravesicular membrane surface. In both models, iron is distributed among a minimum of two and perhaps three types of sites on the intravesicular surface (S_i, S_j, S_k). In addition, differences between first-order rate constants arise from intra- and intermolecular interactions involving the iron-binding moieties as well as a transmembrane electron transfer protein and may include the forward and reverse iron translocation rates. The effect of DCCD is of a kinetic origin resulting from binding to a subunit of the transmembrane electron transfer protein (Vuokila & Hassinen, 1990) and/or may result from disruption of iron binding equilibria or conformational coupling to an H^+-ATPase proton channel which may be identical to S_j as suggested by our preliminary results (Li et al., 1991a).

It is possible to suggest two types of models for the sequence of reactions occurring after iron dissociation from transferrin. Reduction may follow Fe(III) transfer from Tf to multiple sites on the intravesicular surface or reduction of Fe(III) at homogeneous sites precedes intramolecular Fe(II) transfer to other sites. Both sequences of events or variations of these sequences can be incorporated into the schemes shown in Figure 7. On the basis of our preliminary results (Li et al., 1991b; Watkins et al., 1992), the electron transfer reactions per se and mobilization rate (k_m of Figure 7) are assumed to be very fast, and the proteins are arranged in large multimolecular complexes in both cases. In addition, preliminary observations of the membrane potential and temperature dependence of ascorbate-mediated mobilization, ascorbate uptake rates for endosomes, and the uptake of iron by endosomes from extravesicular chelators suggest that the first-order rate constants for ascorbate (k_t, k_{-t}, or V_{max}) may be assigned to translocation (Watkins et al., 1992; Escobar et al., 1992). The first-order rate constants for NADH (k_a, k_{a*}, or V_{max}) may be preliminarily assigned to processes involved in electron transfer from acceptor A to donor D of the transmembrane electron transfer protein. The first-order rate constants for ferrocyanide (k_p, k_{-p}, or V_{max}) may be preliminarily assigned to configurational rearrangements (K_p, $K_{p'}$, or $K_{p''}$) of the multimolecular protein complexes. Alternatively, if configurational rearrangements are fast, the rate constants for ferrocyanide can be assigned to intramolecular iron transfer (k_{ji} or k_{kj}). On the basis of the differences between apparent iron binding sites as detected by the reductants, the models where Fe(III) transfer between sites occurs before reduction are favored.

In general, both schemes are attractive on the basis of available data, however, differences among the amounts of iron mobilized are not well understood. Factors which may contribute to the control of iron mobilization may include vesicle heterogeneity, intermolecular protein–protein interactions, intramolecular conformational changes, iron transfer between low-affinity iron binding moieties, and electron transfer between oxidation–reduction sites with favorable redox potentials including the mobilizable iron. Although the relative roles of these kinetic and thermodynamic factors on iron mobilization are not known at this time, it is reasonable to suggest that they may be operationally significant. Overall, these results and considerations indicate the complexity of endocytic membrane processes with regards to iron transport and provide insights into avenues for further investigation that may allow better characterization of iron uptake by reticulocytes.

REFERENCES

Arai, H., Berne, M., & Forgac, M. (1987) *J. Biol. Chem. 262*, 11006–11011.

Cantor, C. R., & Schimmel, P. R. (1980) *Biophysical Chemistry*, Part III, pp 907–916, W. H. Freeman and Company, San Francisco.

Choe, H. R., Mosely, S. T., Glass, J., & Nunez, M. T. (1987) *Blood 70*, 1035–1039.

Cleland, W. W. (1963) *Biochim. Biophys. Acta 67*, 104–137.

Crane, F. L., Sun, I. L., Clark, M. G., Grebing, C., & Low, H. (1985) *Biochim. Biophys. Acta 811*, 233–264.

Eigen, M., & de Maeyer, L. (1963) *Tech. Org. Chem.* 793–894.

Escobar, A., Gaete, V., & Nunez, M. T. (1992) *J. Bioenerg. Biomembr.* (in press).

Faller, L. D., Diaz, R. A., Scheiner-Bobis, G., & Farley, R. A. (1991) *Biochemistry 30*, 3503–3510.

Fersht, A. (1977) *Enzyme Structure and Function*, pp 118–121, W. H. Freeman and Company, San Francisco.

Fersht, A., & Requena, Y. (1971) *J. Mol. Biol. 60*, 279–290.

Fox, J. B., Nicholas, R. A., Ackerman, S. A., & Swift, C. E. (1974) *Biochemistry 13*, 5178-5186.
Frost, A. A., & Pearson, R. G. (1953) Kinetics and Mechanism, pp 173-177, John Wiley & Sons, New York.
Glass, J., & Nunez, M. T. (1986) *J. Biol. Chem. 261*, 8298-8302.
Honkakoski, P. J., & Hassinen, I. E. (1986) *Biochem. J. 237*, 927-930.
Iacopetta, B. J., & Morgan, E. H. (1983) *J. Biol. Chem. 258*, 9108-9115.
Li, C.-Y., Hamazaki, S., Watkins, J. A., Altazan, J. D., & Glass, J. (1991a) *FASEB J. 5*, A749.
Li, C.-Y., Watkins, J. A., & Glass, J. (1991b) *Blood 78*, 87a.
Nunez, M. T., & Glass, J. (1985) *J. Biol. Chem. 260*, 14707-14711.
Nunez, M. T., Cole, E. S., & Glass, J. (1983) *J. Biol. Chem. 258*, 1146-1151.
Nunez, M. T., Pinto, I., & Glass, J. (1989) *J. Membr. Biol. 107*, 129-135.
Nunez, M. T., Gaete, V., Watkins, J. A., Glass, J. (1990) *J. Biol. Chem. 265*, 6688-6692.
Segel, I. H. (1975) *Enzyme Kinetics*, pp 560-590, John Wiley & Sons, New York.
Sun, I. L., Crane, F. L., Grebing, C., & Low, H. (1984) *J. Bioenerg. Biomembr. 16*, 583-595.
Sun, I. L., Navas, P., Crane, F. L., & Morre, D. J., & Low, H. (1987) *J. Biol. Chem. 262*, 15915-15921.
Thorstensen, K. (1988) *J. Biol. Chem. 263*, 16837-16841.
Vuokila, P. T., & Hassinen, I. E. (1988) *Biochem. J. 249*, 339-344.
Vuokila, P. T., & Hassinen, I. E. (1989) *Biochim. Biophys. Acta 974*, 219-222.
Wang, C. S. (1977) *Eur. J. Biochem. 78*, 569-574.
Wang, C. S. (1980) *Biochim. Biophys. Acta 616*, 22-29.
Watkins, J. A., Nunez, M. T., Gaete, V., Alvarez, O., & Glass, J. (1990) *J. Membr. Biol. 119*, 141-149.
Watkins, J. A., Altazan, J. D., Elder, P., Gaete, V., Li, C.-Y., Nunez, M. T., & Glass, J. (1992) *FASEB J. 6*, A190.

Fluorescence-Detected Assembly of the Signal Recognition Particle: Binding of the Two SRP Protein Heterodimers to SRP RNA Is Noncooperative†

Fabiola Janiak,‡ Peter Walter,§ and Arthur E. Johnson*,‡

Department of Chemistry and Biochemistry, University of Oklahoma, Norman, Oklahoma 73019, and Department of Biochemistry and Biophysics, University of California, San Francisco, California 94143-0448

Received December 30, 1991; Revised Manuscript Received April 1, 1992

ABSTRACT: Protein–RNA and protein–protein interactions involved in the assembly of the signal recognition particle (SRP) were examined using fluorescence spectroscopy. Fluorescein was covalently attached to the 3′-terminal ribose of SRP RNA following periodate oxidation, and the resulting SRP RNA-Fl was reconstituted into a fluorescent SRP species that was functional in promoting translocation of secretory proteins across the membrane of the endoplasmic reticulum. Each of the two protein heterodimers purified from SRP elicited a substantial change in fluorescein emission upon association with the modified RNA. The binding of SRP9/14 to singly-labeled SRP RNA-Fl increased fluorescein emission intensity by 41% at pH 7.5 and decreased its anisotropy from 0.18 to 0.16. The binding of SRP68/72 increased the fluorescein anisotropy from 0.18 to 0.23 but did not alter the emission intensity of SRP RNA-Fl. These fluorescence changes did not result from a direct interaction between the dye and protein because the fluorescein remained accessible to both iodide ions and fluorescein-specific antibodies in the complexes. The spectral changes were elicited by specific SRP RNA–protein interactions, since (i) the SRP9/14- and SRP68/72-dependent changes were unique, (ii) an excess of unlabeled SRP RNA, but not of tRNA, blocked the fluorescence changes, and (iii) no emission changes were observed when SRP RNA-Fl was titrated with other RNA-binding proteins. Each heterodimer bound tightly to the RNA, since the K_d values determined spectroscopically and at equilibrium for the SRP9/14 and the SRP68/72 complexes with SRP RNA-Fl were <0.1 and 7 ± 3 nM, respectively. The binding affinity of SRP68/72 for SRP RNA-Fl was unaffected by the presence of SRP9/14, and hence the binding of the heterodimers to SRP RNA is noncooperative in the absence of SRP54 and SRP19. The SRP protein heterodimers therefore associate randomly and independently with SRP RNA to form domains in the particle that are distinct both structurally and functionally. Any cooperativity in SRP assembly would have to be mediated by SRP54 and/or SRP19.

In eukaryotic cells, proteins destined for secretion and those destined to be integral membrane proteins are initially synthesized on cytoplasmic ribosomes. A nascent chain of such a protein is recognized when its signal sequence emerges from the ribosome and is bound to a ribonucleoprotein complex termed the signal recognition particle (SRP)[1] [Walter et al., 1981; for a review, see Walter and Lingappa (1986)]. The association of SRP with the ribosomal complex slows further

† This work was supported by National Institutes of Health Grants GM 26494 (A.E.J.) and GM 32384 (P.W.).

* Address correspondence to this author at the Department of Chemistry and Biochemistry, University of Oklahoma, 620 Parrington Oval, Norman, OK 73019.
‡ University of Oklahoma.
§ University of California.

[1] Abbreviations: SRP, signal recognition particle; SRP RNA-Fl, SRP RNA with a fluorescein dye covalently attached to the 3′-terminal ribose; ER, endoplasmic reticulum; SDS, sodium dodecyl sulfate; PAGE, polyacrylamide gel electrophoresis.

0006-2960/92/0431-5830$03.00/0